# A study of transition from n- to p-type based on hexagonal $WO_3$ nanorods sensor*

Wu Ya-Qiao(武雅乔), Hu Ming(胡 明)†, and Wei Xiao-Ying(韦晓莹)

*School of Electronics and Information Engineering, Tianjin University, Tianjin* 300072, *China*

(Received 6 July 2013; revised manuscript received 17 October 2013; published online 20 February 2014)

Hexagonal $WO_3$ nanorods are fabricated by a facile hydrothermal process at 180 °C using sodium tungstate and sodium chloride as starting materials. The morphology, structure, and composition of the prepared nanorods are studied by scanning electron microscopy, X-ray diffraction spectroscopy, and energy dispersive spectroscopy. It is found that the agglomeration of the nanorods is strongly dependent on the PH value of the reaction solution. Uniform and isolated $WO_3$ nanorods with diameters ranging from 100 nm–150 nm and lengths up to several micrometers are obtained at PH = 2.5 and the nanorods are identified as being hexagonal in phase structure. The sensing characteristics of the $WO_3$ nanorod sensor are obtained by measuring the dynamic response to $NO_2$ with concentrations in the range 0.5 ppm–5 ppm and at working temperatures in the range 25 °C–250 °C. The obtained $WO_3$ nanorods sensors are found to exhibit opposite sensing behaviors, depending on the working temperature. When being exposed to oxidizing $NO_2$ gas, the $WO_3$ nanorod sensor behaves as an n-type semiconductor as expected when the working temperature is higher than 50 °C, whereas, it behaves as a p-type semiconductor below 50 °C. The origin of the n- to p-type transition is correlated with the formation of an inversion layer at the surface of the $WO_3$ nanorod at room temperature. This finding is useful for making new room temperature $NO_2$ sensors based on hexagonal $WO_3$ nanorods.

**Keywords:** hexagonal, $WO_3$ nanorods sensor, hydrothermal method, n- to p-type transition

**PACS:** 07.07.Df, 61.62.Fk, 78.67.Qa **DOI:** 10.1088/1674-1056/23/4/040704

## 1. Introduction

Nanostructure metal–oxide semiconductor materials such as nanowires, nanorods, and nanotubes have attracted increasing attention in gas sensing applications because of their excellent performances, owing to their large surface-to-volume ratio, lower electron recombination rate, high stability, and less agglomerated configuration.[1–3] Among various nanostructure metal–oxide semiconductor materials, tungsten trioxide ($WO_3$) nanorod/nanowire is a highly promising candidate for $NO_2$, which is the major factor in the production of acid rain, smog, and the depletion of the ozone layer.[4] However, $WO_3$ has several polymorphs with triclinic, monoclinic, orthorhombic, tetragonal and hexagonal structures of this kind of oxide. In these various crystal structures, monoclinic $WO_3$ nanostructure sensors have been extensively studied.[5–11] They exhibit a high sensitivity to $NO_2$ but at the expense of high power consumption because of high operating temperature about 100 °C–300 °C. Thus, it is significant to explore the response of a sensor based on the tungsten-oxide nanostructure at room temperature for low-power gas sensing applications. Therefore, in the last decade, there have appeared some room temperature gas sensors based on the tungsten-oxide nanostructure, more importantly, some of them have exhibited transition from n- to p-type behavior by adjusting their work temperatures.[12–15] Solis *et al.*[13] reported that a mixture of monoclinic and tetragonal phases of $WO_3$ nanocrystalline was made by evaporation of tungsten metal and the film sensor showed excellent sensing properties upon exposure to a low concentration of $H_2S$ in air at room temperature. Kim *et al.*[14] reported that nonstoichiometric monoclinic $WO_{2.72}$ nanowires were produced by thermal decomposition of $W(CO)_6$ and the as-prepared sensor showed an n-type behavior at temperatures above 150 °C and a p-type behavior at temperatures below 100 °C upon exposure to ethanol. Our previous research[15] reported that Ti-added nonstoichiometric monoclinic $W_{18}O_{49}$ nanowires were synthesized by the solvothermal method and the sensor behaves as an n-type semiconductor at operating temperatures above 100 °C and a p-type below 100 °C versus of $NO_2$. However, for $NO_2$ there are few reports on the transition from an n- to a p-type of hexagonal $WO_3$ nanowires/nanorods sensor induced by lowing working temperature.

In this work, firstly, uniform and isolated $WO_3$ nanorods are synthesized at PH = 2.5 by adjusting the PH value and the corresponding energy dispersive spectroscopy (EDS) spectra of the samples are examined. Secondly, the structures and morphologies of the raw $WO_3$ nanorods obtained at PH = 2.5 and the annealed samples are characterized using X-ray diffraction (XRD) and scanning electron microscopy (SEM).

*Project supported by the National Natural Science Foundation of China (Grant Nos. 60771019, 61271070, and 61274074) and the Tianjin Key Research Program of Application Foundation and Advanced Technology, China (Grant No. 11JCZDJC15300).

†Corresponding author. E-mail: huming@tju.edu.cn

© 2014 Chinese Physical Society and IOP Publishing Ltd 

Thirdly, the gas sensing properties of the $WO_3$ nanorod sensor are examined for $NO_2$ in dry air at the working temperatures from 25 °C to 250 °C. Finally, we further examine the gas dynamic responses of the $WO_3$ nanorod gas sensor to some reducing gases including $CH_3OH$, $C_2H_5OH$, and $C_3H_8O$ at room temperature. The results clearly show that the gas sensor behaves as an n-type semiconductor at operating temperatures higher than 50 °C, whereas as a p-type below 50 °C. To the best of the authors' knowledge, this is the first report on the hexagonal $WO_3$ nanorod sensor exhibiting two completely different $NO_2$-sensing responses. This finding has great significance for developing low power consumption $NO_2$ sensors based on hexagonal $WO_3$ nanorods.

## 2. Experiment

### 2.1. Synthesis of $WO_3$ nanorods

$WO_3$ nanorods were synthesized through hydrothermal technology. In a typical procedure, 3.30-g $Na_2WO_4{\cdot}2H_2O$ and 1.17-g NaCl were dissolved in 75 mL of deionized water. $Na_2WO_4{\cdot}2H_2O$ served as the precursor and was used without further purification. NaCl was used as a structure directing agent (SDA), which has been proven to facilitate the controllable growth of nanostructure $WO_3$. The pH value of the solution was adjusted using a 3-M HCl solution. The mixture was then transferred into a Teflon-lined stainless steel autoclave and heated at 180 °C for 24 h. In this experiment, all reagents were purchased from Guangfu Fine Chemical Research Institute (Tianjin, China).

### 2.2. Characterization

The morphology, crystal structure, and element composition of the $WO_3$ nanorods are characterized using a field emission scanning electron microscope (FESEM) ( FEI Nanosem 430), XRD (RIGAKU D/MAX 2500V/PC, Cu K$\alpha$ radiation), and EDS attached on the FESEM.

### 2.3. Sensor fabrication and $NO_2$ response measurement

Firstly, the gas sensors were fabricated by spin coating the slurry of as-prepared tungsten-oxide nanorods on the cleaned alumina substrates which were attached with a pair of interdigital Pt electrodes and followed by a thermal treatment at 300 °C for 2 h in order to burn out the organic solvent used in the preparation of coating slurry and to enhance the adherence of the sensing film to the sensor substrates. Then, the gas sensing characteristics of the as-prepared sensor were measured in a static gas sensing testing system,[15,16] which was composed of a test chamber, a flat heating plate, a professional digital multi-meter, a data acquisition system, and a digital temperature controller. The operating temperature was changed from room temperature to 250 °C by adjusting the digital temperature controller, and the resistance change of the sensor was monitored by a UNITUT70D professional digital multi-meter. A schematic diagram of the measurement system is shown in Fig. 1.

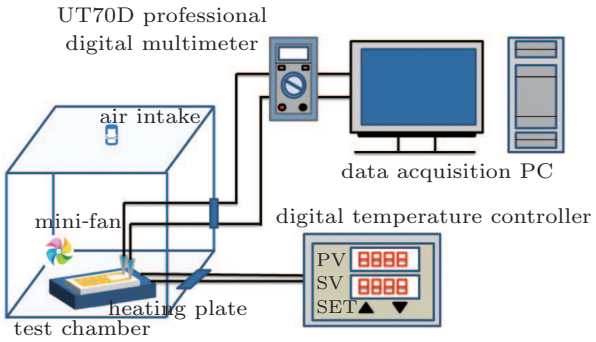



**Fig. 1.** (color online) Schematic diagram of the gas-sensing measurement system.

When being exposed to $NO_2$, the sensor response presents an n-type feature at working temperatures above 50 °C and a p-type feature below 50 °C. Hence, the sensitivity is defined as $S = R_g/R_a$ above 50 °C and as $S = R_a/R_g$ below 50 °C, where $R_a$ and $R_g$ are the resistances of the sensor element in the atmospheric air and the target gas respectively. The time taken by the sensor to achieve 90% of the total resistance change is defined as the response and recovery time.

## 3. Results and discussion

### 3.1. Morphology and structure

We first examine the influences of the PH value, varying from 1.4 to 3.0, on the sample morphology. The SEM images of the $WO_3$ samples obtained at different PH values are shown in Figs. 2(a)–2(e). When the PH value decreases to the values in a range of 1.4–1.9, the obtained $WO_3$ nanorods aggregate each other, resulting in the formation of bundle structures (Figs. 2(a) and 2(b)). The nanorods began to separate from others when the PH value is increased to 2.1–2.3 (Figs. 2(c) and 2(d)). Lots of uniform and isolated $WO_3$ nanorods can be obtained at a PH value of 2.5, where nanorods are randomly oriented and separated from each other and their lengths are in the range 3 μm–5 μm and cross sections in the range 100 nm–150 nm (Fig. 2(e)). However, for the samples prepared at PH = 3, we do not find any precipitate. This may be explained by the disappearance of $H_2WO_4$ in this condition according to the growth mechanism of $WO_3$ nanorods.

The growth mechanism of $WO_3$ nanorods can be explained according to the following reactions:[17,18]

$$Na_2WO_4 + HCl \rightarrow H_2WO_4 + NaCl, \quad (1)$$

$$H_2WO_4 \rightarrow WO_3(\text{crystalnucleus}) + H_2O, \quad (2)$$

$$WO_3(\text{crystalnucleus}) \rightarrow WO_3(\text{nanorods}). \quad (3)$$

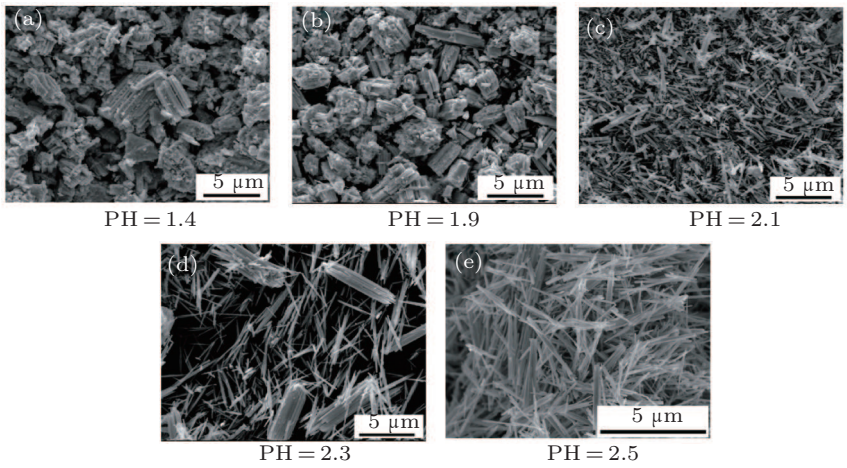



**Fig. 2.** SEM images of the $WO_3$ samples obtained at pH = 1.4 (a), 1.9 (b), 2.1 (c), 2.3 (d), and 2.5 (e).

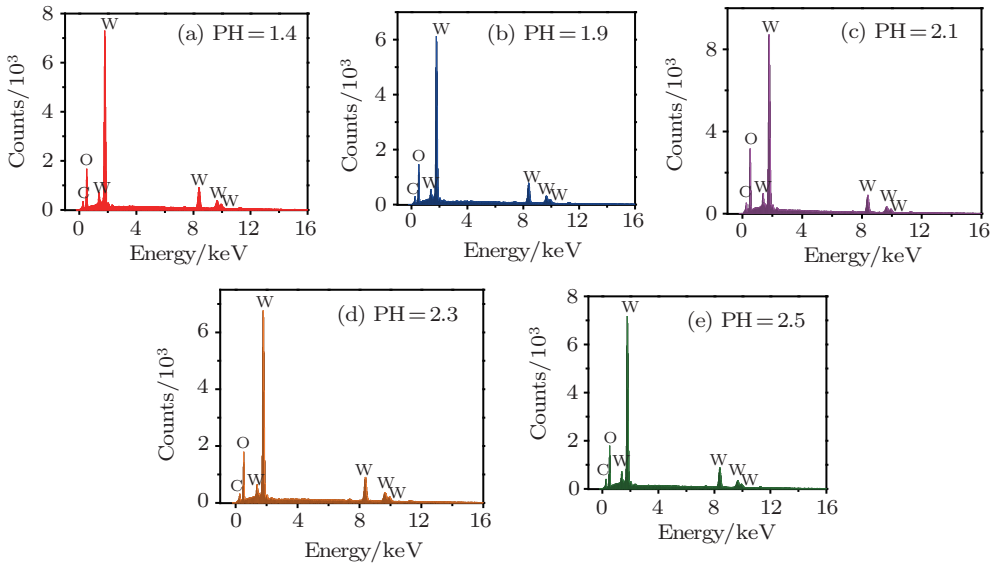



**Fig. 3.** (color online) EDS spectra of the $WO_3$ samples obtained at pH =1.4 (a), 1.9 (b), 2.1 (c), 2.3 (d), and 2.5 (e).

The formation of $H_2WO_4$ is conducible to the growth of $WO_3$ nanorods. Further, the PH acts as the protonation–deprotonation balance of surface hydroxylated groups of growth units, and hence, as the electrostatic surface charge.[19] Similar observations were made by Gu *et al.*[20] and Zheng *et al.*[18] Gu *et al.*[20] obtained bundles at $1.0 < \text{pH} < 1.4$ and isolated rods for $1.5 < \text{pH} < 2.0$; Zheng *et al.*[18] obtained bundles at $2.0 < \text{pH} < 2.2$ and isolated rods for $2.3 < \text{pH} < 2.4$. These results show the importance of PH in the hydrothermally grown $WO_3$ nanorods. Hence, the PH value of resolution is fixed at 2.5 for the later study. The corresponding EDS spectra of the samples are shown in Fig. 3. The EDS spectra show the atomic concentrations of W and O to be 22.13 and 75.62% at PH = 1.4, 22.28% and 75.74% at PH = 1.9, 20.64% and 77.56% at PH=2.1, 21.09% and 76.94% at PH = 2.3, 21.37% and 75.98% at PH = 2.5. The EDS analysis shows the atomic ratio between W and O is close to 1:3. The C element in the EDS can be attributed to originating from the conductive tapes.

In order to identify whether there is any influence of thermal treatment at 300 °C for 2 h on morphologies and crystal structures of $WO_3$ nanorods, we measured XRD spectra and took the SEM images of the $WO_3$ nanorods before and after annealing, and these results are demonstrated in Figs. 4(a) and 4(b).

The main diffraction peaks of the freshly-obtained $WO_3$ nanorods and the annealed nanorods can be well indexed to a hexagonal $WO_3$ with lattice parameters of $a = 0.7298$ nm, $b = 0.7298$ nm, $c = 0.3899$ nm, (JCPDS No. 75-2187). Thus, the crystal structure of $WO_3$ nanorods is still of the hexagonal phase before and after annealing. In the XRD pattern, the (200) diffraction peak has the strongest reflection, indicating that the (200) is the preferential growth plane of the nanorods. The crystallite sizes of $WO_3$ nanorods are estimated using the

Scherrer equation based on the (200) peak, and they are found to be 22.87 nm and 27.93 nm before and after annealing. Consequently, the crystallite size increases when it is under thermal treatment. A further examination in Fig. 4(b), besides the peaks of hexagonal $WO_3$ and corundum $Al_2O_3$, shows that three small diffraction peaks appear at 28.000, 40.096, and 46.403, which are corresponding to tetragonal $W_5O_{14}$ (401), monoclinic $WO_{2.83}$ ($\bar{3}16$), and $WO_{2.92}$ ($\bar{2}030$) plane that can be seen clearly. These are due to the fact that they have lots of oxygen vacancies compared with $WO_3$. According to the relevant literature,[12–15,21] we suppose that the existence of monoclinic $WO_{2.83}$, $WO_{2.92}$, and tetragonal $W_5O_{14}$ are helpful to improve the gas sensing properties at room temperature. In addition, we can see that the morphology of $WO_3$ nanorods is not changed by thermal treatment, as shown in the inset of Fig. 4.

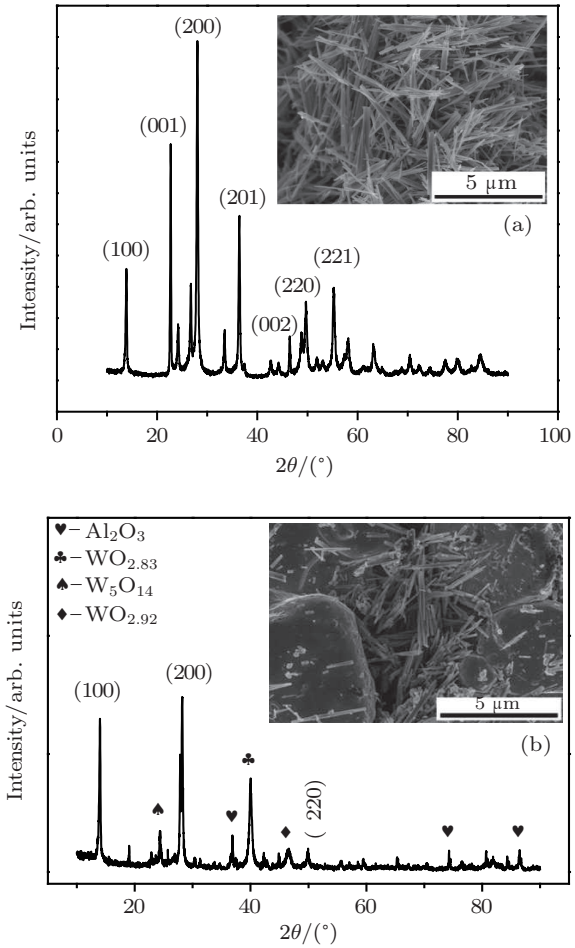



**Fig. 4.** XRD patterns and SEM images of (a) the as-produced $WO_3$ nanorods before annealing, and (b) the $WO_3$ nanorod film coated on $Al_2O_3$ after annealing at 300 °C for 2 h.

### 3.2. Gas-sensing properties

The adsorption, diffusion, and surface reaction rates between the target gas and the gas sensing layer can be influenced by the operating temperature, which will further affect the sensor response. Therefore, we first investigate the optimum operating temperature for the $WO_3$ nanorod sensor by sensing 1-ppm $NO_2$ from room temperature to 250 °C. Metal oxides-based gas sensors are classified into n-type and p-type according to whether they show a decrease or an increase of conductivity when they are exposed to an oxidizing gas (such as $NO_2$).[22,23] As shown in Fig. 5, the $WO_3$ nanorod sensor shows a different sensing behavior. The $WO_3$ nanorod film shows a p-type response at temperatures in the range 25 °C–50 °C, and it shows an n-type response at temperatures in the range 50 °C–250 °C. The sensitivity of the $WO_3$ nanorod sensor operated at room temperature to 1-ppm $NO_2$ is 1.7 and the sensitivity of the sensor decreases with the operating temperature increasing from 25 °C–50 °C. The sensitivity of the sensor increases with the operating temperature increasing from 50 °C to 200 °C and then decrease as the operating temperature increases further. The reason is that at lower operating temperatures (50 °C–200 °C), sufficient thermal energy is essential to overcome the activation energy barrier; however, when the operating temperature is too high (250 °C), the desorption process becomes dominant. Furthermore, the diffusion depth becomes lower at a high temperature.[24] The maximum response reaches about 2.3 at 200 °C.

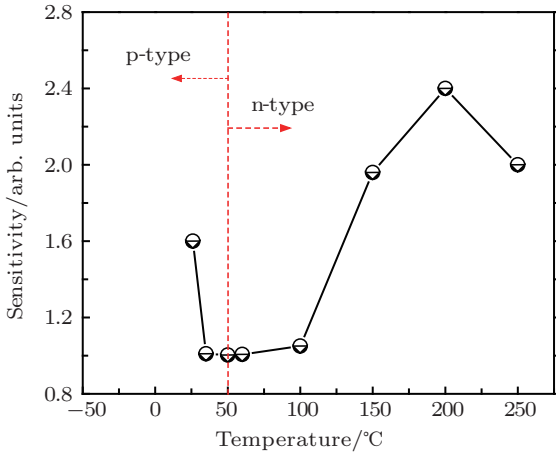



**Fig. 5.** (color online) Variations of the gas sensing sensitivity of $WO_3$ nanorod film to 1-ppm $NO_2$ gas with different working temperatures.

Owing to the fact that the $WO_3$ nanorod sensor shows two different sensing behaviors by changing the working temperature, in order to obtain further clues to the kinetic behavior of $NO_2$ on the $WO_3$ nanorod sensor surface, a second set of experiments is carried out in which the $NO_2$ concentration is increased in a number of steps from 500 ppb up to 5 ppm at optimum operating temperatures of 200 °C and 25 °C, as shown in Figs. 6 and 7.

Turn to the case of higher temperature (200 °C) interactions first. Figure 6 shows that at 200 °C, the resistance is observed to increase as the sensor is exposed to $NO_2$, indicating that the $WO_3$ nanorod sensor behaves as an n-type semiconductor and the sensor shows that the response is enhanced with the increase of gas concentration. Remarkably, very little baseline drift occurs after the final concentration of $NO_2$

(i.e., 5 ppm) has been reached. On the whole, $NO_2$ undergoes a reversible oxidizing interaction with the $WO_3$ nanorod film surface. It is accepted that upon being exposed to $NO_2$ gas, the $NO_2$ gas molecules are absorbed at the active sites on tungsten-oxide nanorods surface and form chemisorbed $NO_2^-$. The process of the reactions can be described as follows:

$$NO_2(gas) + e^- \rightarrow NO_2^-(ads), \quad (4)$$

$$NO_2(gas) + O_2^-(ads) + e^- \rightarrow NO_2^-(ads) + 2O^-(ads). \quad (5)$$

The above reactions reduce the electron concentration on the material surface, increase the width of the depletion layer and finally result in an increase of the sensor resistance. When the $NO_2$ concentration is increased, the number of electrons extracted from the conduction band and the barrier in the conduction band of $WO_3$ is also increased. As a result, the electrical resistance and the sensitivity are both increased. In order to reveal the moments of the gas input and gas stop, the enlarged part of data in Fig. 6(a) measured at an $NO_2$ concentration of 3 ppm is illustrated in Fig. 6(b) and the response time and recovery time are 136 s and 175 s respectively.

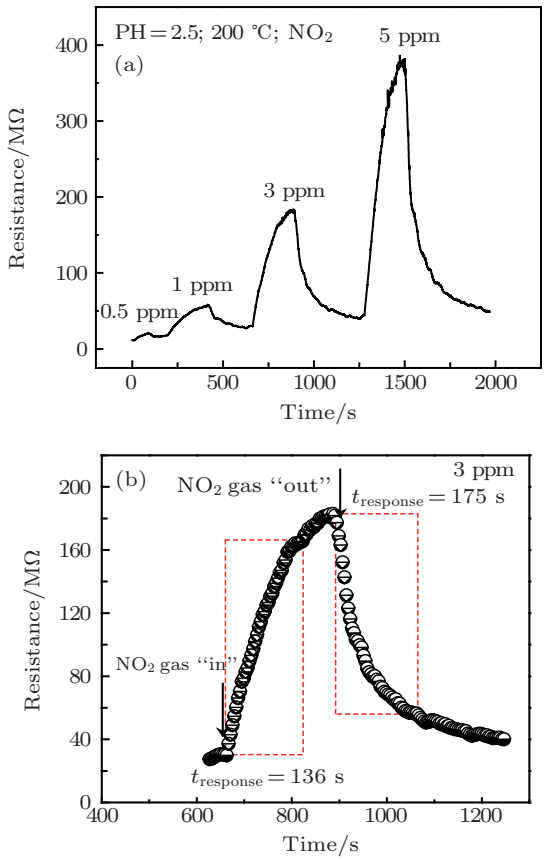



**Fig. 6.** (color online) (a) Dynamic response resistances of $WO_3$ nanorod film to 0.5, 1, 3, and 5-ppm $NO_2$ gas at 200 °C. (b) Enlarged part of (a): the $WO_3$ nanorod film at 3-ppm $NO_2$.

Now, we come to the case of room-temperature interactions; the n-type behavior, however, changes completely when the experiments of the same kind are carried out again after the surface temperature has been reduced to room temperature. Figure 7 shows that a decrease in the sensor resistance is observed instead of the expected resistivity increasing when being exposed to $NO_2$ and the sensor also shows that the response is enhanced with the increase of gas concentration. Figure 7(b) shows the enlarged part of the data in Fig. 7(a), measured at an $NO_2$ concentration of 1 ppm, to reveal the moments of the gas input and gas stop, and the response time and recovery time are 40 s and 160 s respectively. The response time and recovery time are both shorter than those shown in Fig. 6(b), indicating that this $WO_3$ nanorod film is a good room temperature gas sensing material.

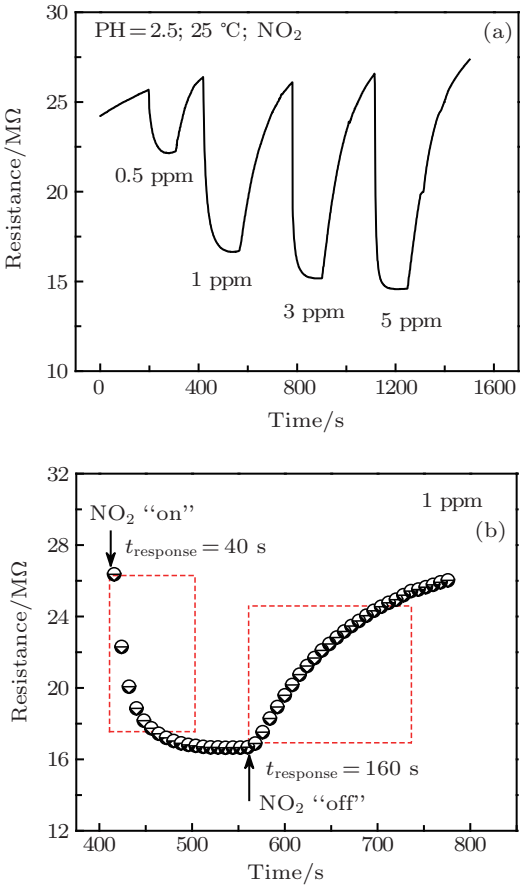



**Fig. 7.** (color online) (a) Dynamic response resistances of $WO_3$ nanorod film to 0.5, 1, 3, and 5-ppm $NO_2$ gas at room temperature. (b) Enlarged part of (a): the $WO_3$ nanorod film at 1-ppm $NO_2$.

The transitions from an n- to a p-type response (or *vice versa*) resulting from the gas concentration or the operating temperature are observed for different metal–oxide semiconductors exposed to various gases.[25–31] One of the conceivable mechanisms for the p-type conductive behavior appearing at room temperature is the formation of an inversion layer at the surface of the $WO_3$ nanorod. Because there are a large number of surface states which are induced by dangling, structural defects, and gas adsorption, the surface of the semiconductor is composed of a surface layer and the space charge layer. For the large density of surface states, the surface layer

with an excess charge leads to an aggregation layer, depletion layer, or even inversion space-charge layer below the surface layer of the semiconductor. For example, in the case of an n-type semiconductor, if the excess charge is a negative charge, the electrostatic potential will be increased in the space charge layer with respect to electrons, and thus the depletion layer is formed. Furthermore, if the excess negative charges are much more, the electrostatic potential will be reduced in the space charge layer with respect to holes, and thus the inversion space-charge layer is formed.

According to the XRD pattern of Fig. 4(b), there is a mixture phase of hexagonal $WO_3$, non-stoichiometry monoclinic $WO_{2.83}$, $WO_{2.92}$, and tetragonal $W_5O_{14}$, which has a large number of oxygen vacancies. The formation of a typical oxygen vacancy might be represented by the following quasi-chemical reaction (6) as reported in Ref. [32]:

$$O_O^* \longleftrightarrow \frac{1}{2}O_2(\text{gas}) + V_O^{2+} + 2e^-, \tag{6}$$

where $O_O^*$ represents an unstable oxygen atom at an oxygen site, $V_O^{2+}$ represents an oxygen vacancy with a double positive charge. It easily adsorbs the oxygen in air to reach stabilization. When the $WO_3$ nanorod sensor is exposed to air, oxygen molecules can be absorbed on the surface of the $WO_3$ nanorod and form chemisorbed oxygen species by capturing electrons from the adsorption sites on the oxide surface. As mentioned above, an inversion space charge layer is formed, in which holes become the main charge carriers.

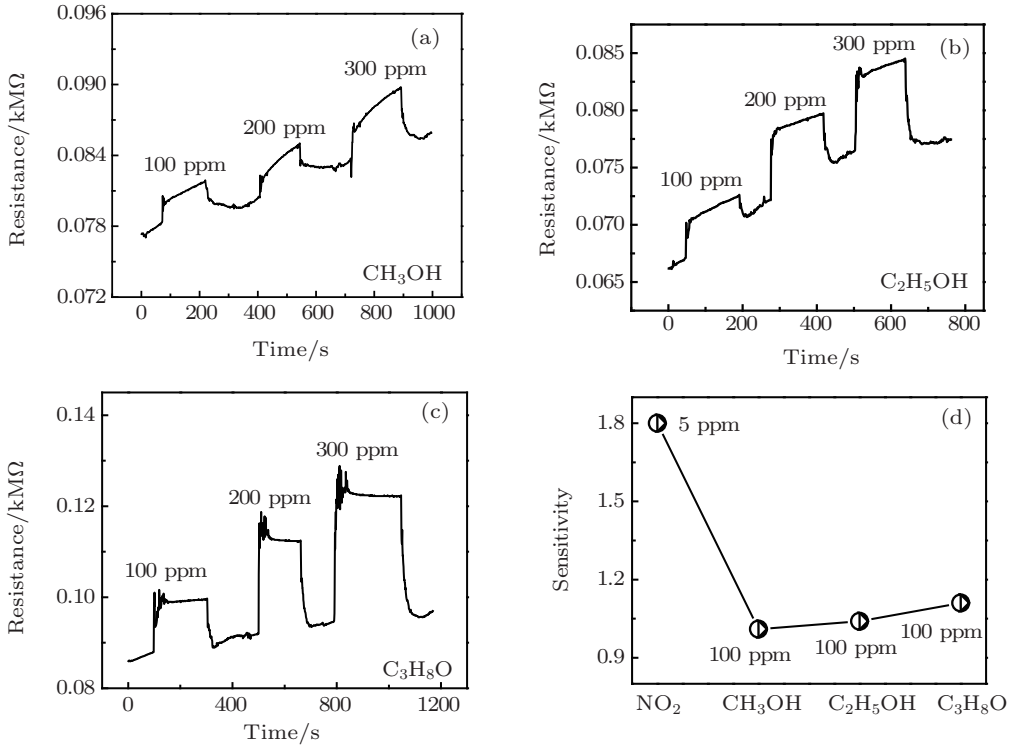



**Fig. 8.** Gas dynamic responses of the $WO_3$ nanorod gas sensor to some reducing gases including $CH_3OH$, $C_2H_5OH$, and $C_3H_8O$ at room temperature.

In order to testify whether the transition from n-type to p-type of $WO_3$ nanorods is an occasional phenomenon at room temperature, we further examine the gas dynamic response of the $WO_3$ nanorod gas sensor to some reducing gases including $CH_3OH$, $C_2H_5OH$, and $C_3H_8O$ at various concentrations from 100 ppm to 300 ppm, as shown in Fig. 8. It can be seen that the $WO_3$ nanorod gas sensor also behaves as a p-type semiconductor since the sensor resistance increases upon the introduction of reducing gas ($CH_3OH$, $C_2H_5OH$, and $C_3H_8O$), indicating that this transition does not take place occasionally. Figure 8(d) shows the comparison among the sensitivities of the $WO_3$ nanorod gas sensor to 5-ppm $NO_2$, 100-ppm $CH_3OH$, 100-ppm $C_2H_5OH$, and 100-ppm $C_3H_8O$, and the sensor exhibits the largest response to 5-ppm $NO_2$ in the other gases, showing that the sensor has a rather good selectivity to $NO_2$ compared with other examined gases at room temperature.

## 4. Conclusion

Uniform and isolated $WO_3$ nanorods can be synthesized at PH = 2.5 through hydrothermal technology. The gas-sensing properties of the $WO_3$ nanorod sensor are examined at 200 °C and room temperature respectively. The n- to p-type conductivity is converted by changing the operating temperature. One conceivable mechanism for the p-type conductive behavior appearing at room temperature is the formation of an inversion layer at the surface of the $WO_3$ nanorod due to the existence of

monoclinic $WO_{2.83}$, $WO_{2.92}$, and tetragonal $W_5O_{14}$ impurity phases. The $WO_3$ nanorod gas sensor also behaves as a p-type semiconductor when being exposed to some reducing gases ($CH_3OH$, $C_2H_5OH$, and $C_3H_8O$). Since the room temperature gas sensing properties of hexagonal $WO_3$ are very promising, it is advisable to study hexagonal $WO_3$ further as a room temperature gas sensor.

## References


[1] Wongchoosuk C, Wisitsoraat A, Phokharatkul D, Horprathum M, Tuantranont A and Kerdcharoen T 2013 *Sens. Actuators B* **181** 388
[2] He J, Su Y M, Ma Y T, Chen Q, Wang R N, Ye Y, Ma Y and Liang H L 2012 *Chin. Phys. B* **21** 076104
[3] Xia L, Zhong K, Song Y, Lu X, Xu L S, Yan Y, Li H D, Yuan F L, Jiang J Z, Yu D P and Zhang S L 2012 *Chin. Phys. B* **21** 097801
[4] Afzal A, Cioffi N, Sabbatini L and Torsi L 2012 *Sens. Actuators B* **171–172** 25
[5] You L, Sun Y F, Ma J, Guan Y, Sun J M, Du Y and Lu G Y 2011 *Sens. Actuators B* **157** 401
[6] Qin Y X, Hu M and Zhang J 2010 *Sens. Actuators B* **150** 339
[7] Zhang C, Debliquy M, Boudiba A, Liao H and Coddet C 2010 *Sens. Actuators B* **144** 280
[8] Kim S J, Hwang I S, Choi J K and Lee J H 2011 *Thin Solid Films* **519** 2020
[9] Meng D, Yamazaki T, Shen Y, Liu Z and Kikuta T 2009 *Appl. Surf. Sci.* **256** 1050
[10] Cao B, Chen J, Tang X and Zhou W 2009 *J. Mater. Chem.* **19** 2323
[11] Hieu N V, Quang V V, Hoa N D and Kim D 2011 *Curr. Appl. Phys.* **11** 657
[12] Hu M, Liu Q L, Jia D L and Li M D 2013 *Acta Phys. Sin.* **62** 057102 (in Chinese)
[13] Solis J L, Saukko S, Kish L B, Gqanqvist C G and Lantto V 2001 *Sens. Actuators B* **77** 316
[14] Kim Y S, Ha S C, Kim K, Yang H, Choi S Y and Kim Y T 2005 *Appl. Phys. Lett.* **86** 213105
[15] Qin Y X, Sun X B, Li X and Hu M 2012 *Sens. Actuators B* **162** 244
[16] Chen H Q, Hu M, Zeng J and Wang W D 2012 *Chin. Phys. B* **21** 058201
[17] Wang J, Khoo E, Lee S P and Ma J 2009 *J. Phys. Chem. C* **113** 9655
[18] Zheng F, Zhang M and Guo M 2013 *Thin Solid Films* **534** 45
[19] Sonia A, Djaoued Y, Subramanian B, Jacques R, Eri M C, Ralf B and Achour B 2012 *Mater. Chem. Phys.* **136** 80
[20] Gu Z, Li H, Zhai T, Yang W, Xia Y, Ma Y and Yao 2007 *J. Solid State Chem.* **180** 98
[21] Balázsi C, Sedlácková K, Llobet E and Ionescu R 2008 *Sens. Actuators B* **133** 151
[22] Moseley P T 1997 *Meas. Sci. Technol.* **8** 223
[23] Williams D E 1999 *Sens. Actuators B* **57** 1
[24] Bai S, Zhang K, Luo R, Li D, Chen A and Liu C C 2012 *J. Mater. Chem.* **22** 12643
[25] Kim Y S, Hwang I S, Kim S J, Lee C Y and Lee J H 2008 *Sens. Actuators B* **135** 298
[26] Gurlo A, Barsan N, Oprea A, Sahm M, Sahm T and Weimar U 2004 *Appl. Phys. Lett.* **85** 2280
[27] Galatsis K, Cukrov L, Wlodarski W, McCormick P, Kalantar-zadeh K, Comini E and Sberveglieri G 2003 *Sens. Actuators B* **93** 562
[28] Dräger G, Czolbe W and Leiro J A 1992 *Phys. Rev. B* **45** 8283
[29] Zhang C, Debliquy M, Boudiba A, Liao H and Coddet C 2010 *Sens. Actuators B* **144** 280
[30] Siciliano T, Tepore A, Micocci G, Genga A, Siciliano M and Filippo E 2009 *Sens. Actuators B* **138** 207
[31] Ruhland B, Becker Th and Muller G 1998 *Sens. Actuators B* **50** 85
[32] Prasad A K, Kubinski D J and Gouma P I 2003 *Sens. Actuators B* **93** 25